Homogenization of periodic 1-3 piezocomposite using wave propagation: Toward an experimental method

Antoine Balé, Rémi Rouffaud, Franck Levassort, Renald Brenner, Anne-Christine Hladky

Homogenization of periodic 1-3 piezocomposite using wave propagation: toward an experimental method

Antoine Balé,[1,a] Rémi Rouffaud,[1,b] Franck Levassort,[1] Renald Brenner,[2] and Anne-Christine Hladky-Hennion[3]

[1]*GREMAN UMR7347, University of Tours, CNRS, INSA-CVL, 37100 Tours, France*

[2]*Sorbonne Université, CNRS, UMR 7190, Institut Jean Le Rond ∂'Alembert, F-75005 Paris, France*

[3]*CNRS, Centrale Lille, ISEN, Univ-Lille, Univ-Valenciennes, UMR8520-IEMN, 59000 Lille, France*

(Dated: 17 May 2021)

1-3 piezocomposites are first choice materials for integration in ultrasonic transducers due to their high electromechanical performance, particularly in their thickness mode. The determination of a complete set of effective electroelastic parameters through a homogenization scheme is of primary importance for their consideration as homogeneous. This allows for the simplification of transducer design using numerical methods. The method proposed is based on acoustic wave propagation through infinite piezocomposite that are considered homogeneous material. Christoffel tensor components for the 2mm symmetry were expressed to deduce slowness curves in several planes. Simultaneously, slowness curves of a numerical phantom were obtained using a Finite Element Method (FEM). Dispersive curves were initially calculated in the corresponding heterogeneous structure. Subsequent identification of the effective parameters was based on a fitting process between the two sets of slowness curves. Then homogenized coefficients were compared with reference results from a numerical method based on fast-Fourier transform (FFT) for heterogeneous periodic piezoelectric materials in the quasi-static regime. A relative error of less than 2% for a very large majority of effective coefficients was obtained. As the aim of the manuscript is to implement an experimental procedure based on the proposed homogenization scheme in order to determine the effective parameters of the material in operating conditions, it is shown that simplifications to the procedure can be performed and that a careful selection of only seven slowness directions is sufficient to obtain the complete database for a piezocomposite containing square shaped fibers. Finally, further considerations to adapt the present work to a 1-3 piezocomposite with fixed thickness are also presented.

[a]Also at CNRS, Centrale Lille, ISEN, Univ-Lille, Univ-Valenciennes, UMR8520-IEMN, 59000 Lille, France
[b]remi.rouffaud@univ-tours.fr

I. INTRODUCTION

Piezoelectric composite materials are used in various applications such as sensors, actuators and transducers. Among the many patterns of spatial distribution between the piezoelectric and inert phases, 1-3 connectivity, i.e., aligned piezoelectric rods embedded in a polymer matrix[1] for the corresponding piezocomposite (13PC), can deliver very high performance in the thickness mode[2], leading to their application in ultrasonic transducers[3]. In order to design transducers integrating 13PCs, numerical methods such as Finite Difference Method (FDM) or Finite Element Method (FEM) are commonly used. However, owing to the complexity of the studied system (number of phases, phase arrangement, microstructure), tedious meshing is required when performing detailed modeling of 13PC. Moreover, depending on the target application the high precision levels achieved by such calculations are not always necessary. Users of numerical methods preferentially model these transducers with a 13PC simulated as a single-phase homogeneous material with effective properties. This theoretical step corresponding to a homogenization procedure is performed in the framework of the long-wavelength approximation and a subject that was extensively studied during the 1980s and 90s when piezocomposites, in particular, 13PC first became available. Typically, models were initially developed for purely elastic materials and subsequently extended to take into account the different coupling phenomena, in particular piezoelectricity.

The simplest approaches are those of Voigt[4] and Reuss[5] with uniform trial fields. These have been extended to piezoelectricity to obtain rigorous upper and lower bounds on the effective free-energy[6]. In 1985, Banno derived an analytical expression for the calculation of several effective material parameters for 13PC[7], based on the model developed by Newnham[1]. Smith *et al.*[2] in addition, considered thickness mode effective parameters of 13PC with analytical expressions. Other workers managed to determine additional effective parameters for all components of the three elastic, dielectric and piezoelectric tensors (electroelastic moduli) for the different piezocomposites[8–11]. However, the accuracy delivered for all parameters related to the thickness mode in these later approaches were not always congruent and very often remained proprietary, in particular parameters for 13PC.

At the end of the 1950's, Eshelby had considered the problem of an ellipsoidal inclusion embedded in an infinite matrix and had obtained the analytical expression of the stress and strain fields which turned out to be unchanged within the inclusion[12]. This fundamental result today forms the basis of several mean-field micromechanical models used to estimate the overall elastic moduli tensor. In 1980, Deeg[13] extended this solution to the calculation of coupled fields, in particular, piezoelectric materials. Dunn and Taya[14] proposed a method of obtaining effective parameters of a piezocomposite, as did various other workers[15–17]. In these configurations, 13PCs are a particular case of these models where one of the axes of ellipsoidal inhomogeneities tends toward infinity. FEM or more generally numerical methods are also used for 13PC homogenization. The main advantage of numerical methods is that there is no restriction on geometry, size, material parameters and number of phases in the structure[18]. With these methods, different boundary conditions (displacement and electrical potential) are applied to the Representative Volume Element (RVE) in order to determine mechanical and electrical fields inside the material. Details of such methods are given in several reports[19–26]. Recently, the various homogenization methods presented above have also been adapted and applied to study novel 13PC in order to demonstrate their enhanced properties[27,28]

For all these models, the required input data are properties of the constituent phases and according to one of the methods briefly described above, this can vary from only a few parameters to the full set of electroelastic moduli for the piezoelectric phase. The effective parameters obtained by these homogenization procedures are therefor directly dependent upon these initial data. However, various 13PC fabrication processes (such as the "Dice and Fill" method[29]) introduce possible variations of properties for each phase and as a consequence variation on the final effective properties. Two examples can be highlighted: the machining process of the piezoelectric phase (starting typically from a bulk ceramic) to design the rods can degrade the piezoelectric properties while addition of the polymer around the rods introduces porosity (air bubbles) which modifies its mechanical properties. Beyond the development of accurate models, measurement of the piezocomposite parameters in *operating conditions* is essential. Characterization based on 13PC electrical impedance measurements was performed by us[30] and the objective of this present work is to develop a homogenization procedure based on acoustic wave propagation. This theoretical procedure was implemented with the understanding that it could then be applied by adapting it to an experimental set-up and thereby effects a correct estimation of homogenized parameters in *operating conditions*.

This approach used mechanical wave propagation through the 13PC and allowed extraction of the effective parameters in a similar way to reported works for different configurations[31–35].

This method as extended to piezoelectric materials, was inspired by Langlet *et al.*[36] who determined the effective tensor of porous elastic materials.

With the assumption of an infinite piezoelectric material, the behavior of wave propagation is first presented for the two media of interest in section II. Then, in section III, slowness curves from homogeneous media are fitted on heterogeneous media with the analytical determination of some elastic parameters before optimization algorithms were used to deliver all the components of the effective electroelastic moduli. From this fit, a homogeneous equivalent medium is determined. In section IV, these results are compared with effective electroelastic coefficients obtained with a Fourier transform-based numerical scheme for periodic piezoelectric materials in the quasi-static regime[37–40]. The same initial database for our numerical phantom was used. This comparison was essential and allowed us to validate our new procedure. The influences of two rod shapes and piezoelectric phase volume fractions on several effective parameters are discussed. Finally, with reference to experimental procedure, two essential points are addressed. First, minimization of the number of slowness values is examined while simultaneously maintaining accuracy on the deduced effective parameters. Finally, considerations aimed at adapting the present work to a piezoelectric medium with a given thickness and lateral dimensions, is put forward.

II. WAVE PROPAGATION IN AN INFINITE PIEZOELECTRIC MATERIAL

For a piezoelectric material, constitutive equations interacts the mechanical parameters (strain S and stress T tensors) with the electrical parameters (electric field E and electric displacement D). In the framework of linear behavior, combining Maxwell equations and

Hooke's law, the interaction is written as follow[41]:

$$\begin{aligned} T_{ij} &= c^E_{ijkl} S_{kl} - e_{ikl} E_i \\ D_i &= \epsilon^S_{ij} E_j + e_{ikl} S_{kl} \end{aligned} \tag{1}$$

where c^E, e and ϵ^S are, respectively, the elastic tensor at constant electric field, the piezoelectric tensor and the dielectric tensor at constant strain and subscripts $i, j, k, l \in [1, 2, 3]$, the 3 space dimensions. Spatial directions 1, 2 and 3 are used indifferently throughout the text with directions X, Y and Z. In the long wavelength approximation, an anisotropic heterogeneous medium can be considered as an anisotropic homogeneous medium if size inhomogeneities are smaller than the selected wavelength[42]. With this assumption, the use of classical plane waves for the study of homogeneous medium in section II B is possible.

A. Heterogeneous structure

To study the wave propagation in a 13PC, FEM is used.

1. FE model: 4mm- and mm2-structures

In this work, two 13PC designs are investigated. The two were chosen because, from a practical point of view, both can be manufactured by the well-known "Dice and Fill" method[29]. In fig.1, top views of the two periodic configurations are shown with grey piezoelectric square-shaped rods (fig.1.**(a)**)[29] or right-triangle (fig.1.**(b)**)[45] shaped rods surrounded by polymer. To determine the effective symmetry of each structure, the rod-shaped piezoelectric material and the relative positionning of rods to each other, are taken into ac-

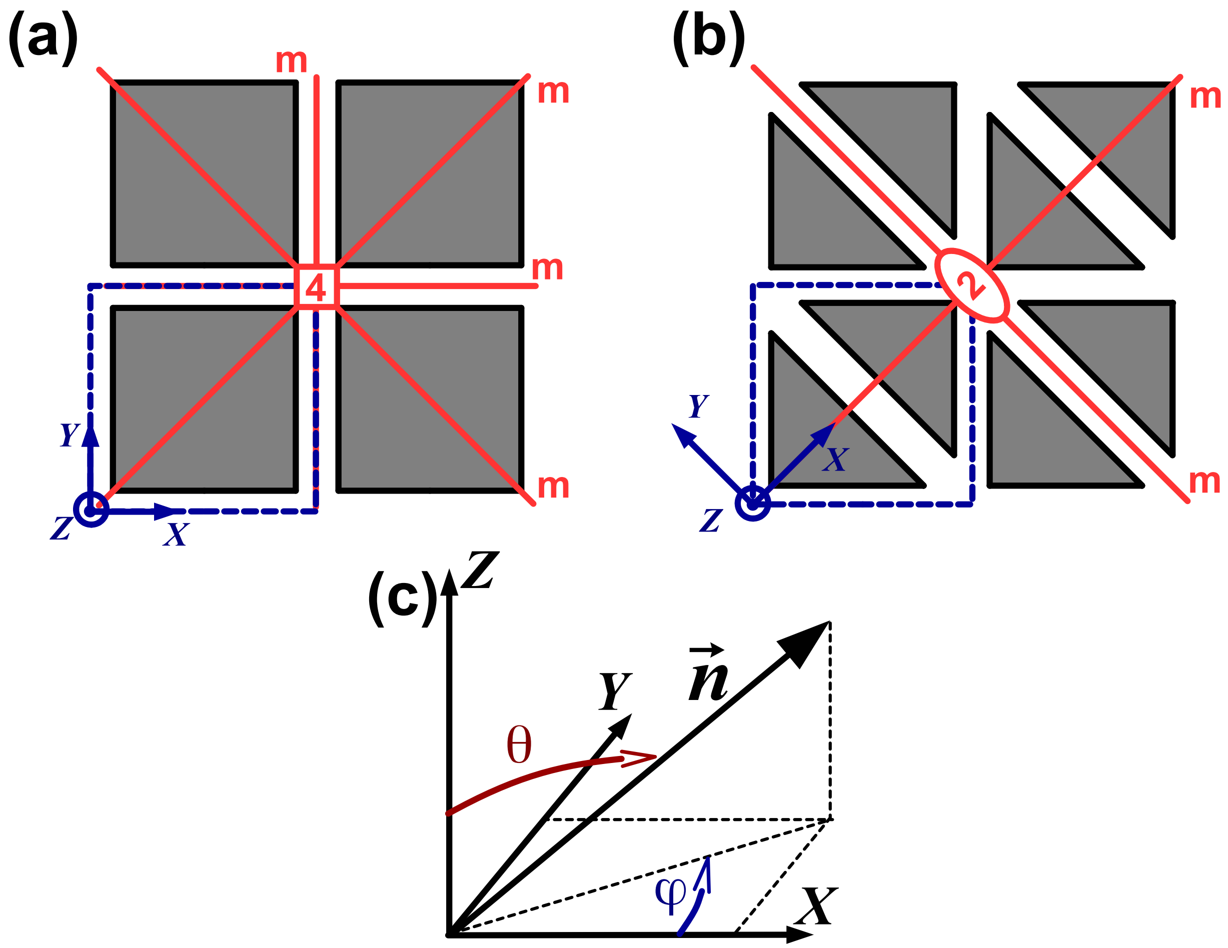

FIG. 1. Top view of elementary 13PC patterns for **a)** 4mm and **b)** mm2 symmetries. Surrounded in blue line, are RVEs meshed with FEM with the local orthonormal basis (XYZ). **c)** Unit propagation vector $\vec{n}$ is defined by angles θ and φ in the local basis. Grey areas represent the piezoelectric rods surrounded by a polymer.

count. In the case of Fig1.**(a)**, 4-fold axis of symmetry exists (red square at center of the representation[42]). In the case of Fig1.**(b)**, it is a 2-fold axis (red ellipse at center of the representation[42]). In both cases, two symmetry planes exist (as represented in the structures, fig.1). Accordingly, the square rods structure has 4mm symmetry while the right-triangle rods structure has mm2 symmetry. These symmetries are dependent on the piezoelectric

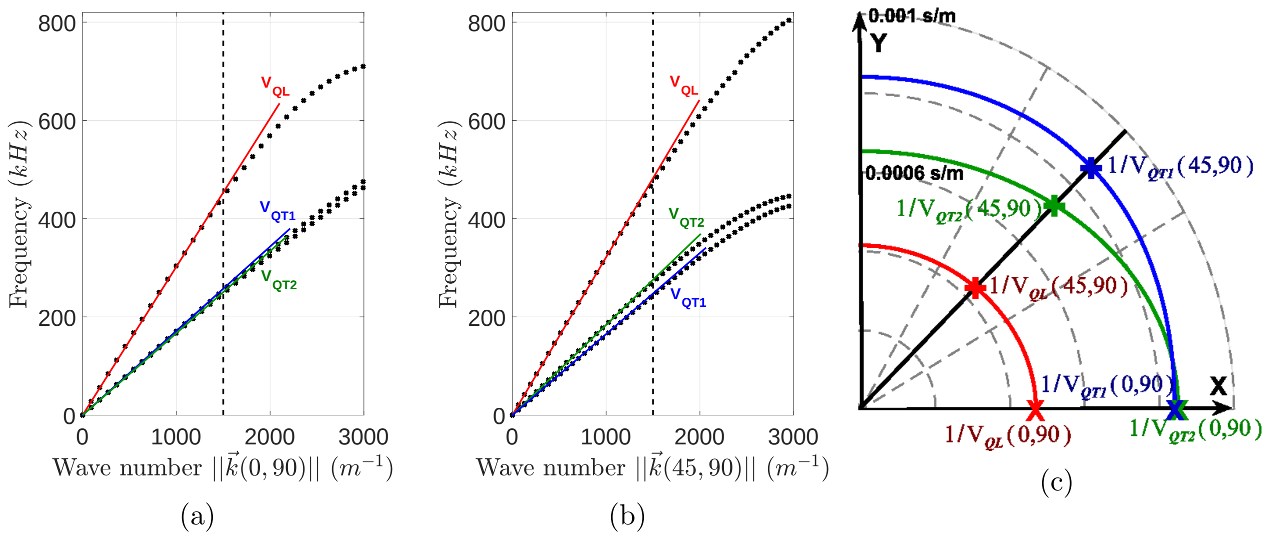

FIG. 2. Dispersion curves in the mm2-structure for 2 different wave vectors (a) $\vec{k}(0,90)$, colinear to $\vec{k_x}$ and (b) $\vec{k}(45,90)$. (c) The final slowness curves for $\|\vec{k}\| = 50\text{m}^{-1}$, $0° < \varphi < 90°$ and $\theta = 90°$. V_{QL}, V_{QT1} and V_{QT2} are group velocities for, respectively, quasi-longitudinal, first quasi-transversal and second quasi-transversal modes. Calculation is performed with PZT-4[43] and Epoxy resin[44] for a 1mm-side RVE and a piezoelectric volume fraction $v_f = 50\%$.

material used for rods (here, the standard 6mm-symmetry ceramic). Parallelepipedic RVEs of each structure are represented in Fig1 for both cases as blue dotted lines. These RVEs possess the same symmetry as that defined previously for the two structures. To respect the orthotropic axis of 13PC, for the mm2 structure, local basis (OXYZ) is rotated through 45° from the local axis of the 4mm structure. Moreover, the unit propagation vector $\vec{n}$ is defined by the angles θ and φ in the local basis (fig.1.**(c)**) and n_1 (resp. n_2, n_3) is the projection of $\vec{n}$ on X-axis (resp. Y-axis, Z-axis):

$$n_1 = sin\theta cos\varphi,\ n_2 = sin\theta sin\varphi,\ n_3 = cos\theta. \tag{2}$$

For the FEM calculations, ATILA software was used[46]. The whole problem domains are divided into elements connected by nodes, where constitutive equations are locally approximated. 1mm-side RVE is chosen. In fact, this is a typical size in XY-plane for 13PC in medical application. The reader is reminded that there is no variation of phases in the z-direction, so the size has no effect on the final results. Isoparametric elements are used with quadratic interpolation along the element's sides. Hexahedrons are used with 20 nodes (8 for the corners and 12 for the middle of the edge) for the 4mm-structure. Similarly, prisms are used with 15 nodes (6 for the corners and 9 for the middle of the edge) for the mm2-structure. Furthermore, the finite element formulation used in ATILA relying upon quadratic interpolation functions, the classical $\lambda/4$ criterion must be verified in the whole mesh to ensure the validity of the finite element result. The $\lambda/4$ states that the largest length of each element in a given mesh has to be smaller than a quarter of the wavelength in the material for the working frequency. For structures studied in this paper, the mesh has been chosen in order to respect this criterion. Moreover, the study of periodic 13PC structure is greatly simplified by the Bloch-Floquet theorem because only one RVE needs to be meshed[36].

2. From dispersion curves to slowness curves

To establish slowness curves for our two studied structures, properties of PZT-4[43] and Epoxy resin[44] in table II were chosen for the two 13PC phases. Dispersion curves were initially calculated for a 1mm-side RVE with a piezoelectric volume fraction of 50% and only the 3 lowest modes in frequency to be in accordance with the long wavelength approximation.

Dispersion curves were calculated for one specific direction of a wave vector in the first Brillouin zone using modal analysis. Wave vector $\vec{k}$ is defined by $\vec{k}(\varphi,\theta) = k_x.\vec{n_1} + k_y.\vec{n_2} + k_z.\vec{n_3}$, where:

- $\varphi \in [-180°, 180°]$,

- $\theta \in [0°, 180°]$ and if $\theta = 90°$, $\vec{k} \in (XY)$-plane,

In fig.2, an example of how the slowness curves are determined is put forward for two specific propagation directions in the XY-plane ($\vec{k}(0,90)$ and $\vec{k}(45,90)$) and for the mm2-structure with a step of 91m^{-1} for $||\vec{k}||$. Specifically, it is shown in fig.2**(a)** and fig.2**(b)**, the quasi-longitudinal (QL), first quasi-transverse (QT1) and second quasi-transverse (QT2) modes, where QT1 (resp. QT2) mode has an out-plane (resp. in-plane) transverse polarization in the studied plane (here, the $XY-$plane). A linear behavior exists at low frequency for the three modes where the phase velocity is equal to the group velocity (V_{QL},V_{QT1},V_{QT2}). Calculating dispersion curves for the whole characteristic volumetric region due to mm2 symmetries ($0° < \varphi < 90°$ and $0° < \theta < 90°$), the limit of this linear region is approximatively $\|\vec{k}\| \simeq$ 1500m^{-1}. This limit is indicated in fig.2**(a)** and **(b)** with the vertical dotted line. To stay within this volumetric linear region, $\|\vec{k}\|$ was fixed to 50m^{-1} for the rest of the study. In fig.2**(c)**, final slowness curves (inverse of velocities) are displayed for one quarter of the XY-plane ($0° < \varphi < 90°$ and $\theta = 90°$). The six velocities calculated from fig.2**(a)** and **(b)** are added to slowness curves (crossed points). For FEM calculation, all the slowness points were calculated in this way with a step of 1° for φ and θ.

B. Homogeneous structure

From the numerical slowness curves in the heterogeneous material, analytical slowness curves in a homogeneous material had to be established for a further comparison between the two media. A general case is described for the mm2 structure in the following subsection. As in section II A, the medium was considered to be infinite and comprised of piezoelectric material.

1. *Wave equation in piezoelectric materials*

Starting from the expression of the mechanical strain T_{ij} (eq.1) and removing the electrical potential dependency, the wave equation in a piezoelectric infinite medium can be written[42,47]:

$$\rho\frac{\partial^2 u_l}{\partial t^2} = c^E_{ijkl}\frac{e_{kij}e_{jkl}}{\epsilon^S_{jk}}\frac{\partial^2 u_l}{\partial n_j \partial n_k} \tag{3}$$

where u_i is the component of the mechanical displacement vector $\vec{u}$ on the axis n_i and the time t. ρ is the density of the medium of propagation. In the assumption of a plane wave propagation problem in an infinite medium in the n_j direction and for the eq.(3), a solution can be written as:

$$u_i = u_i^0 e^{j\omega(t-\frac{n_j x_j}{V})} = u_i^0 F(t - \frac{n_j x_j}{V}) \tag{4}$$

where u_i^0 is the wave polarization and V the phase velocity. When this solution is included in eq.3, the wave equation extended to piezoelectric medium becomes:

$$\rho V^2 u_i^0 = (\Gamma_{il} + \frac{\gamma_i \gamma_l}{\epsilon})u_l^0 \tag{5}$$

where $\Gamma_{il} = c^E_{ijkl} n_j n_k$, $\gamma_i = e_{kij} n_j n_k$ and $\epsilon = \epsilon^S_{jk} n_j n_k$. The $(\Gamma_{il} + \frac{\gamma_i \gamma_l}{\epsilon})$ term is called the piezoelectric Christoffel tensor and written as:

$$\overline{\Gamma}_{il} = \begin{bmatrix} \overline{\Gamma}_{11} & \overline{\Gamma}_{12} & \overline{\Gamma}_{13} \\ \overline{\Gamma}_{12} & \overline{\Gamma}_{22} & \overline{\Gamma}_{23} \\ \overline{\Gamma}_{13} & \overline{\Gamma}_{12} & \overline{\Gamma}_{33} \end{bmatrix} \tag{6}$$

Eq.5 is an eigenvalues equation where the wave polarization u^0_l is the eigenvector of $\overline{\Gamma}_{il}$ with its eigenvalue $\lambda = \rho V^2$. As $\overline{\Gamma}_{il}$ is symmetrical, eigenvalues are real and to provide real velocities, eigenvalues must also be positive. Eigenvectors are orthogonal because of the symmetry of $\overline{\Gamma}_{il}$. Therefore, solving eq.5 is equivalent to finding the roots of equation:

$$|\overline{\Gamma}_{il} - \rho V^2 \delta_{il}| = 0 \tag{7}$$

where δ_{il} is the Kronecker symbol. Eq.7 has three solutions for a given propagation direction $\vec{n}$ that are velocities from the 3 known plane waves QL, QT1 and QT2 (i.e., section II A 2).

2. *mm2-structure (right-triangular rods 13PC)*

As mentionned earlier, the most general case is developed in this section. A mm2 piezoelectric material is characterized by 17 independent parameters: 9 elastic coefficients $(c^E_{11}, c^E_{12}, c^E_{13}, c^E_{22}, c^E_{23}, c^E_{33}, c^E_{44}, c^E_{55}, c^E_{66},)$, 5 piezoelectric coefficients $(e_{15}, e_{24}, e_{31}, e_{32}, e_{33},)$ and 3 dielectric parameters $(\epsilon^S_{11}, \epsilon^S_{22}, \epsilon^S_{33},)$. In comparison, a 4mm-structure is described by 5 elastic, 3 piezoelectric and 3 dielectric independent parameters. For both cases, all components of the piezoelectric Christoffel tensors are analytically determined (Appendix A).

From these expressions, velocities V_{QL}, V_{QT1} and V_{QT2} can be determined using eq.7 for any direction. Depending on the symmetry class, calculations for all directions is not always necessary and can be restricted. For a mm2-structure, three planes of propagation are sufficient: XY-plane, XZ-plane and YZ-plane. Solutions for the XY-plane are described in detail here and the two other planes in Appendix B.

In the XY-plane, the components of the projection vector $\vec{n}$ are given by:

$$n_1 = cos\varphi \ , \ n_2 = sin\varphi \ , \ n_3 = 0 \ . \tag{8}$$

A direct consequence of this is the zero value for the $\overline{\Gamma}_{13}$ and $\overline{\Gamma}_{23}$ terms in the Christoffel tensor and a simplification of the expression for $\overline{\Gamma}_{11}$, $\overline{\Gamma}_{12} = \overline{\Gamma}_{21}$, $\overline{\Gamma}_{22}$ and $\overline{\Gamma}_{33}$ components. Consequently, eq.7 is reduced to:

$$\left(\overline{\Gamma}_{33} - \lambda\right) \left[\left(\overline{\Gamma}_{11} - \lambda\right) \left(\overline{\Gamma}_{22} - \lambda\right) - \overline{\Gamma}_{12}^2\right] = 0 \tag{9}$$

where $\lambda = \rho V_i^2$ are eigenvalues. The three solutions of eq.9 are:

$$\begin{cases} \lambda = \overline{\Gamma}_{33} \\ \lambda_{\pm} = \frac{1}{2}\left[\overline{\Gamma}_{11} + \overline{\Gamma}_{22} \pm \sqrt{\left(\overline{\Gamma}_{11} + \overline{\Gamma}_{22}\right)^2 - 4\left(\overline{\Gamma}_{11}\overline{\Gamma}_{22} - \overline{\Gamma}_{12}^2\right)}\right] \end{cases} \tag{10}$$

To assign the solutions to the correct polarizations (i.e., QL, QT1 or QT2 mode), eigenvectors are determined. As an example, one can describe the expression of the simplest solution for the XY-plane is detailed as: $\lambda = \overline{\Gamma}_{33}$. Substituting $\overline{\Gamma}_{33}$ by its definition, the complete expression of the corresponding velocity becomes:

$$V_{QT2}^2 = \frac{1}{\rho}\left[c_{55}^E cos^2\varphi + c_{44}^E sin^2\varphi + \frac{\left(e_{15}cos^2\varphi + e_{24}sin^2\varphi\right)^2}{\epsilon_{11}^S cos^2\varphi + \epsilon_{22}^S sin^2\varphi}\right] \tag{11}$$

Doing the same for V_{QT1} and V_{QL} (with the two other eigenvalue expressions), the slowness curves can be analytically calculated for a homogeneous piezoelectric material in the 3 planes of interest for a mm2 symmetry case.

III. HOMOGENEOUS EQUIVALENT STRUCTURE

The symmetry class of the equivalent homogeneous structure must be the same as the initial heterogeneous structure (here 13PC) and this condition must be taken into account when defining all the components of the $\overline{c}^E$, $\overline{e}$ and $\overline{\epsilon}^S$ tensors. Overlined variables are components of the homogeneous equivalent structure. In general, if the symmetry class is unknown, the most general triclinic class is chosen by default. In the present case, a mm2-symmetry class was retained because right-triangular rods are PZT4 with 6mm-symmetry class. The objective was to deduce all the effective components of the elastic, piezoelectric and dielectric tensors with a comparison of the slowness curves obtained by the two approaches (heterogeneous and homogeneous materials materials) described earlier. This determination of all the parameters is performed in two steps. The first step involves the direct determination of several elastic parameters. A fitting process of slowness curves involving calculation by FEM is described, in a second step(section II A). The two step are detailed below. The homogenization process relies on numerical slowness curves calculated by FEM. The case of the mm2-structure (fig.1**(b)**) with a volume fraction (v_f) of 50% is presented and numerical slowness curves are presented on fig.3.

A. Step 1: analytical determination of elastic constants.

For specific directions in any plane (0°, 45°, 90°), the analytical expressions of velocities (section II B) are simplified to enable the determination of some elastic constants. For instance, in the XY-plane where general equations ($\varphi-$dependence) are given by the system

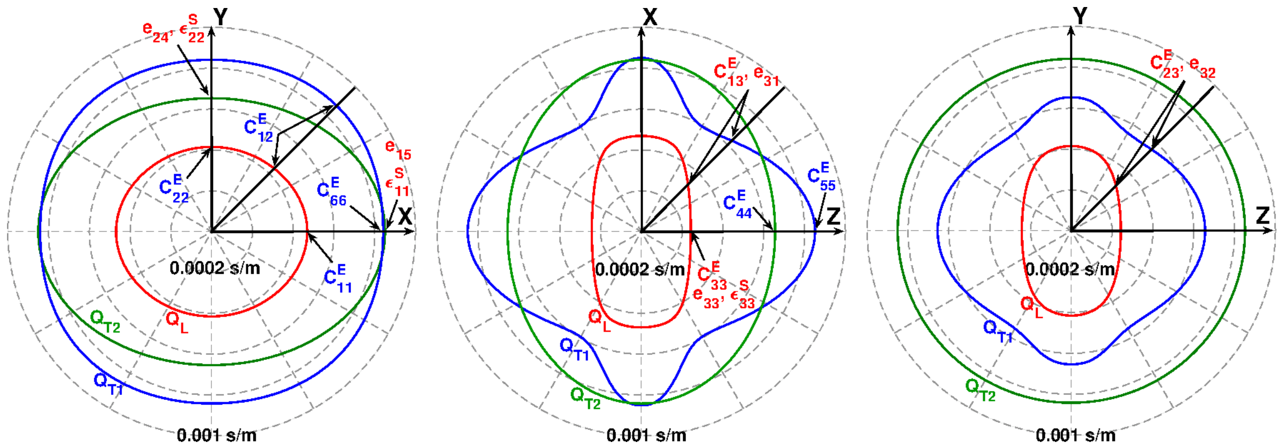

(a) (b) (c)

FIG. 3. Numerical slowness curves for three orthogonal planes from the same mm2-structure. Calculation is performed with PZT-4[46] and Epoxy resin[44] for a 1mm-side RVE and a piezoelectric volume fraction v_f =50%.

(10), and when $\varphi = 0°$ and $\theta = 90°$, velocities are expressed by:

$$\begin{cases} V_{QT2}^2(0,90) = \frac{1}{\rho}\left[\overline{c}_{55}^E + \dfrac{\overline{e}_{15}^2}{\overline{\epsilon}_{11}^S}\right] \\ V_{QT1}^2(0,90) = \frac{\overline{c}_{66}^E}{\rho} \\ V_{QL}^2(0,90) = \frac{\overline{c}_{11}^E}{\rho} \end{cases} \tag{12}$$

From this set of equations the numerical values from dispersion curves (fig.3**(a)**) at $\varphi = 0°$ and $\theta = 90°$, $\overline{c}_{11}^E$ and $\overline{c}_{66}^E$ are easily determined. Similarly, $\overline{c}_{55}^E$ can be resolved in the case of a purely elastic medium ($\overline{e}_{15} = 0$) but by taking into account the piezoelectricity, three unknowns: $\overline{c}_{55}^E$, $\overline{e}_{15}$ and $\overline{\epsilon}_{11}^S$ are added. In a similar way, some elastic constants can be determined for other directions: $\overline{c}_{22}^E$ in the direction $\vec{n}(90,90)$ on the $1/V_{QL}$ curve and $\overline{c}_{12}^E$ in the direction $\vec{n}(45,90)$ on the $1/V_{QL}$ and $1/V_{QT2}$ curves. In general, all elastic constants that can be determined are added to fig.3 in blue color. Other constants that cannot be analytically and independently determined like $\overline{e}_{15}$ and $\overline{\epsilon}^S_{11}$, are shown in red. Finally, $\overline{c}^E_{55}$ is no longer an unknown value because it can be determined in the $\vec{n}(0,0)$ direction ($XZ-$plane) on $1/V_{QT2}$ curve. The same analysis is performed on the $XZ-$ and $YZ-$planes (fig.3). Several effective tensor components appear in different directions but in order not to overload fig.3, these are displayed only once. For example, it can be observed that $\overline{c}^E_{55}$ appears both in the expressions of $V_{QT2}(0,90)$ (system 12) and $V_{QT2}(0,0)$ (fig.3**(b)**). All the six parameters that can be determined analytically are summurized in table I. The same table is applicable for the 4mm-structure, except that the $(90,90)$-direction and the QT1 mode from the $(90,90)$-direction are not necessary, for this symmetry structure.

Finally, for the mm2-symmetry, with three orthogonal planes and six different directions, a system of nine independent equations is achieved with 11 unknowns. Here, the full determination of tensor components is not analytically possible. Consequently, the second step is a numerical determination performed by a fitting process.

B. Step 2: fitting process.

For a full determination of effective tensors, eleven constants have to be fitted: $\overline{c}^E_{13}$, $\overline{c}^E_{23}$, $\overline{c}^E_{33}$, all the five constants of $\overline{e}$ tensor and the three constants of $\overline{\epsilon}^S$ tensor. The fitting process by the objective function (OF) that is minimized and the settings for the optimization algorithm (OA) are described below. Both slowness and velocity are used interchangeably throughout the text because once one is determined, the other one is simultaneously determined too.

TABLE I. Analytical expressions for particular directions used for determining six elastic constants in mm2-structure.

	(φ,θ)	Mode	$\rho V_{QL,QT1,QT2} =$
XY-plane	(0,90)	Q$_L$	$\overline{c}^E_{11}$
		Q$_{T1}$	$\overline{c}^E_{66}$
	(90,90)	Q$_L$	$\overline{c}^E_{22}$
	(45,90)	Q$_L$,Q$_{T1}$	$\frac{A+B}{4} \pm \frac{\left[(A+B)^2 - AB + \left(\overline{c}^E_{12} + \overline{c}^E_{66}\right)^2\right]^{\frac{1}{2}}}{4}$ with $A = \left(\overline{c}^E_{11} + \overline{c}^E_{66}\right)$, $B = \left(\overline{c}^E_{22} + \overline{c}^E_{66}\right)$
XZ-	(0,0)	Q$_{T1}$	$\overline{c}^E_{55}$
		Q$_{T2}$	$\overline{c}^E_{44}$

1. *Objective function*

The aim of this process is to fit the analytical velocities from a homogeneous medium onto numerical velocities considered as the reference from heterogeneous medium. Therefore, one needs to minimize the difference between the numerical velocities $v_{ij_{\text{FEM}}}$ and analytical velocities $v_{ij_{\text{Chris}}}$ for all propagation directions of the three planes of interest for the mm2-symmetry. Specifically, $v_{ij_{\text{FEM}}}$ are gleaned from section II A 2 while $v_{ij_{\text{Chris}}}$ are calculated for each iteration from equations established in section II B 2 with the new set of parameters to be fitted (unknown components of effective tensors). For each new set, a score S_a is calculated by the OF using the least squares method:

$$S_a = \sum_{i=1}^{M} \left(\sum_{j=1}^{N} \frac{\left(v_{ij_{\mathrm{FEM}}} - v_{ij_{\mathrm{Chris}}}\right)^2}{N < v^2_{ij_{\mathrm{FEM}}} >} \right) \tag{13}$$

where M is the number of slowness curves selected for the fitting process ($M = 5$ for the mm2-structure and $M = 3$ for the 4mm-structure) and N is the number of propagation directions used (with a default of $N = 360$). Finally, $<>$ is the mean symbol. The five specific curves (fig.4) were specifically chosen because the remaining unknowns that must be determined are involved in their analytical expressions (see red constants on fig3). 4mm-structure requires fewer slowness curves to be fitted because there are fewer effective independent components, in a similar way to the simplification of table I for this case, as explained earlier.

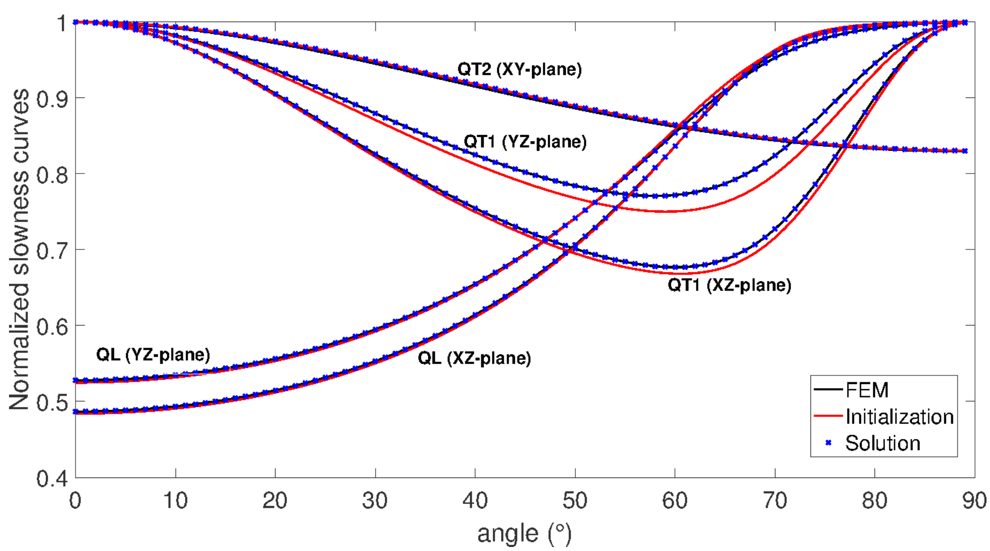

FIG. 4. Selected slowness curves (M=5) for the fitting process displayed on one quarter of the plane (φ,$\theta \in [0° \; 90°]$).

2. Optimization algorithm

The OA selects a new set of parameters based on all previous scores returned by OF for the different sets, previously selected. The time needed to reach the best optimization score is called rate of convergence. In order to achieve a fast convergence rate, an OA based on a canonical search is preferred. Here the Nelder-Mead algorithm[48], also known as the simplex method was used.

In the case of a mm2-structure, the set of effective parameters to be determined is described by the vector $x = \left\{\overline{c}^E_{13}, \overline{c}^E_{23}, \overline{c}^E_{33}, \overline{e}_{31}, \overline{e}_{32}, \overline{e}_{33}, \overline{e}_{24}, \overline{e}_{15}, \overline{\epsilon}^S_{11}, \overline{\epsilon}^S_{22}, \overline{\epsilon}^S_{33}\right\}$. One of the drawbacks of using this kind of OA is the requirement of an initial vector (x_{init}) to start the process. Values of x_{init} are set with the matrix method[11] that provides a good approximation for longitudinal tensor (subscripts $_{33}$) but a weak approximation of the transverse tensors parameters. It is worth mentioning that these values are calculated as a function of the 13PC volume fraction of piezoelectric phase.

The second setting for the algorithm is the definition of the search-space limits. These are contained in the boundary vectors x_{UB} for the upper boundaries and x_{LB} for the lower boundaries. Here, the choice of a large search-space is preferred and boundary vectors are defined by $x_{\text{UB}} = 5x_{\text{init}}$ and $x_{\text{LB}} = 0.01x_{\text{init}}$.

In fig.4, the five selected slowness curves for the fitting process are represented only on one quarter of their planes for the case $v_f = 50\%$. The curves are normalized to their own maximum to highlight the differences. The black curves that almost coincide with the dotted blue lines are the FEM calculations. The red curves are the initial slowness curves of the OA and were calculated using x_{init} in table II.

TABLE II. Case $v_f = 50\%$. Elastic (c^E in GPa), piezoelectric (e in C.m^{-2}), dielectric (ϵ^S in $/\epsilon_0$) constants and density (ρ in kg/m^3) for PZT4[43] ceramic, Epoxy[44] resin, mm2- and 4mm- structures calculated by the present method and by the FFT method. Initial vector x_{init} for the OA and relative differences between FFT and present methods are also given. Star (resp. cross and dash) indicates constants analytically determined on first step (resp. non-value parameter and known parameters from others values).

Constants		c^E_{11}	c^E_{12}	c^E_{13}	c^E_{22}	c^E_{23}	c^E_{33}	c^E_{44}	c^E_{55}	c^E_{66}	e_{15}	e_{24}	e_{31}	e_{32}	e_{33}	ϵ^S_{11}	ϵ^S_{22}	ϵ^S_{33}	ρ
PZT-4		139	77.8	74.3	-	-	115.4	25.6	-	30.6	12.7	-	-5.2	-	15.1	730	-	635	7500
Epoxy resin		7.84	3.9	-	-	-	-	-	-	-	-	-	-	-	-	3	-	-	1100
Constants		$\overline{c}^E_{11}*$	$\overline{c}^E_{12}*$	$\overline{c}^E_{13}$	$\overline{c}^E_{22}*$	$\overline{c}^E_{23}$	$\overline{c}^E_{33}$	$\overline{c}^E_{44}*$	$\overline{c}^E_{55}*$	$\overline{c}^E_{66}*$	$\overline{e}_{15}$	$\overline{e}_{24}$	$\overline{e}_{31}$	$\overline{e}_{32}$	$\overline{e}_{33}$	$\overline{\epsilon}^S_{11}$	$\overline{\epsilon}^S_{22}$	$\overline{\epsilon}^S_{33}$	$\overline{\rho}$
x_{init}		×	×	7.56	×	7.56	40	×	×	×	0.0039	0.0039	-0.27	-0.27	9.15	6	6	333	×
mm2	this work	16.04	8.43	8.28	18.85	9.16	41.50	6.90	4.76	4.98	0.0136	0.0195	-0.33	-0.36	8.69	8	12	332	4300
	FFT	16.28	8.58	8.40	19.12	9.37	40.88	7.00	4.85	5.07	0.0112	0.037	-0.33	-0.40	9.07	10	10	326	-
	rel. dif.(%)	1.54	1.81	1.62	1.41	2.35	1.50	1.47	1.85	1.79	19.3	61.9	0.51	11.6	4.25	18.5	12.2	1.71	-
4mm	this work	19.37	6.37	8.64	-	-	40	5.57	-	3.92	0.0075	-	-0.273	-	9.14	5	-	332	4300
	FFT	19.25	6.39	8.66	-	-	40.73	5.53	-	3.9	0.0167	-	-0.353	-	9.08	9	-	332	-
	rel. dif.(%)	0.62	0.31	0.23	-	-	1.81	0.72	-	0.51	76	-	25.6	-	0.66	57	-	0	-

IV. RESULTS AND DISCUSSION

Homogenization results are presented for two different cases: (1) results for a specific volume fraction (v_f) of 50% for 4mm and mm2 13PC are presented in the first section, (2) parameter variation as a function of v_f are shown in second section. In both sections, all results are compared with the FFT method for validation. The principle of this numerical scheme is briefly recalled in Appendix C.

A. Specific case of $v_f = 50\%$

The volume fraction of $v_f = 50\%$ was chosen because it is a typical 13PC value employed for medical imaging applications. This value allows for the optimization of the thickness coupling coefficient (k_t) which is an essential parameter for transducer design[3]. Variations of v_f are possible (typically between 30% and 90%) depending on the desired optimized properties. Fig.4 shows the solution found by the fitting process (blue dotted lines). The maximum difference between the initialization and the FEM is located on the QL wave in the $XZ-$plane at 62° and its value is 2.98%. After the fitting process, the solution presents a maximum difference on the QT2 wave in the $XY-$plane, equal to 0.3% (equating to 10 fold reduction when compared to x_{init}). It is also noticeable that the curves from the QT2 wave in the $XY-$plane was unchanged between x_{init} and the solution. In fact, this curve is governed by Eq.11. OA can only modify variables $\overline{e}_{24}$, $\overline{e}_{15}$ $\overline{\epsilon}^S_{11}$ and $\overline{\epsilon}^S_{22}$ in this equation as $\overline{c}^E_{44}$ and $\overline{c}^E_{55}$ are already determined and considered fixed values. Essentially, the problem is that, in Eq.11, the term $\frac{\left(e_{15}cos^2\varphi+e_{24}sin^2\varphi\right)^2}{\epsilon^S_{11}cos^2\varphi+\epsilon^S_{22}sin^2\varphi}$ is approximately 500 times smaller than $c_{55}^E cos^2\varphi + c_{44}^E sin^2\varphi$. This means that at least for this case, the variables $\overline{e}_{24}$, $\overline{e}_{15}$, $\overline{\epsilon}_{11}^S$ and $\overline{\epsilon}_{22}^S$ are not highly sensitive. As a result, OA had no influence on them.

In table II, all effective tensor components from the solution are given in the case of the 4mm-structure (fig.1**(a)**) and the mm2-structure (fig.1**(b)**). For compararive purposes, the same components obtained by the FFT method are also presented. As expected from the previous paragraph, large relative differences appear for $\overline{e}_{24}$, $\overline{e}_{15}$ $\overline{\epsilon}_{11}^S$ and $\overline{\epsilon}_{22}^S$ until 62%. However, these differences are not of critical concern because, in practice, these parameters do not affect the expected behavior of 13PC functions either in thickness or flexural modes. To reduce these differences, additional work needs to be performed during OF selection, by for example, adding another slowness curve for the fit or giving extra-weight for this QT2 slowness curve.

B. Results for v_f variations

In this section, the homogenization method is performed on different volume fractions (10%, 30%, 50% and 70%) and compared with the FFT method. In fig.5, the elastic constants calculated from the present study (black crosses) are well evaluated for the most effective constants (< 2%). In fact, the largest relative difference with the FFT method (red circles) appears to be 6% for $\overline{c}_{44}^E$ at $v_f = 70\%$. This difference is not significant when compared with the $\overline{c}_{44}^E$ value of 24% for 4mm-structure (blue crosses). However, these variations of elastic constants show that the shapes have a stronger effect on the constant characteristics of the $x-$axis ($\overline{c}_{11}^E$) as compared with $\overline{c}_{22}^E$ on the $y-$axis and $\overline{c}_{33}^E$ on the $z-$axis.

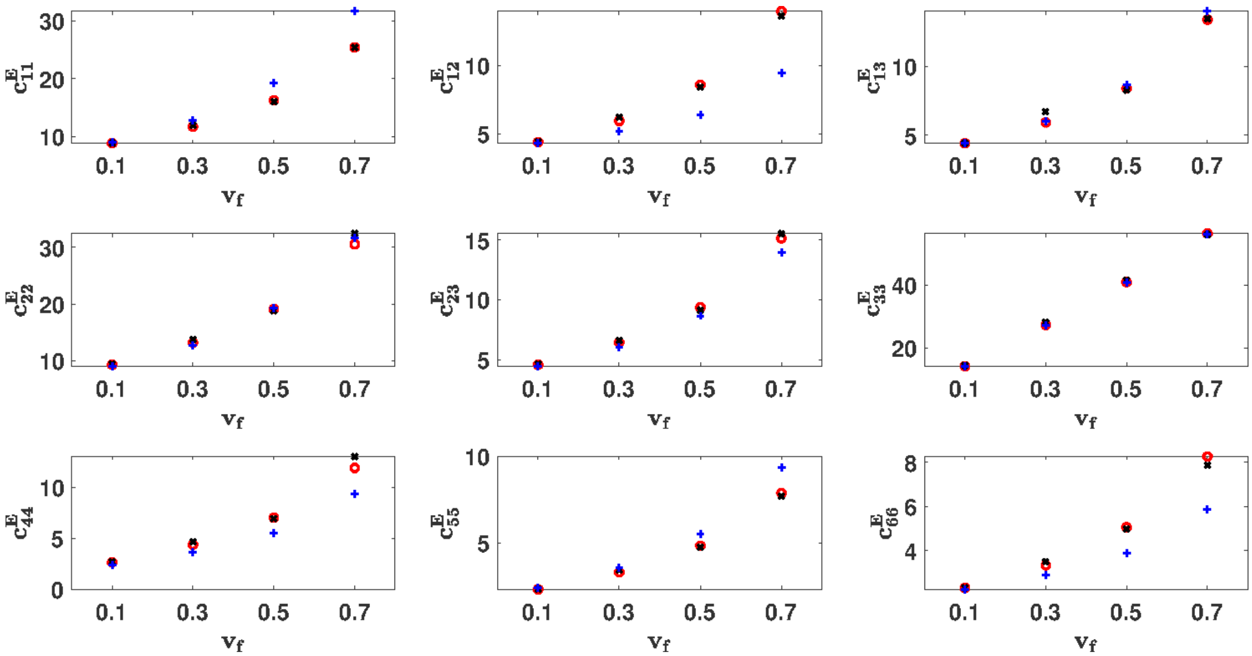

FIG. 5. Effective elastic constants (in GPa) as a function of piezoelectric volume fraction (v_f) from the present study represented with the black cross for mm2-structure and blue plus-sign for 4mm-structure. Results from FFT numerical scheme (red circles) are also added for the mm2-structure.

Fig.6 shows homogenized piezoelectric and dielectric effective parameters. The gap between the FFT and the present method on $\overline{e}_{24}$ and $\overline{e}_{15}$ was unexpectedly negligible for the reasons already explained in paragraph IV A. However, this difference was pronounced for the higher volume fractions. Details on the constants' sensitivity are extensively covered by Balé[47].

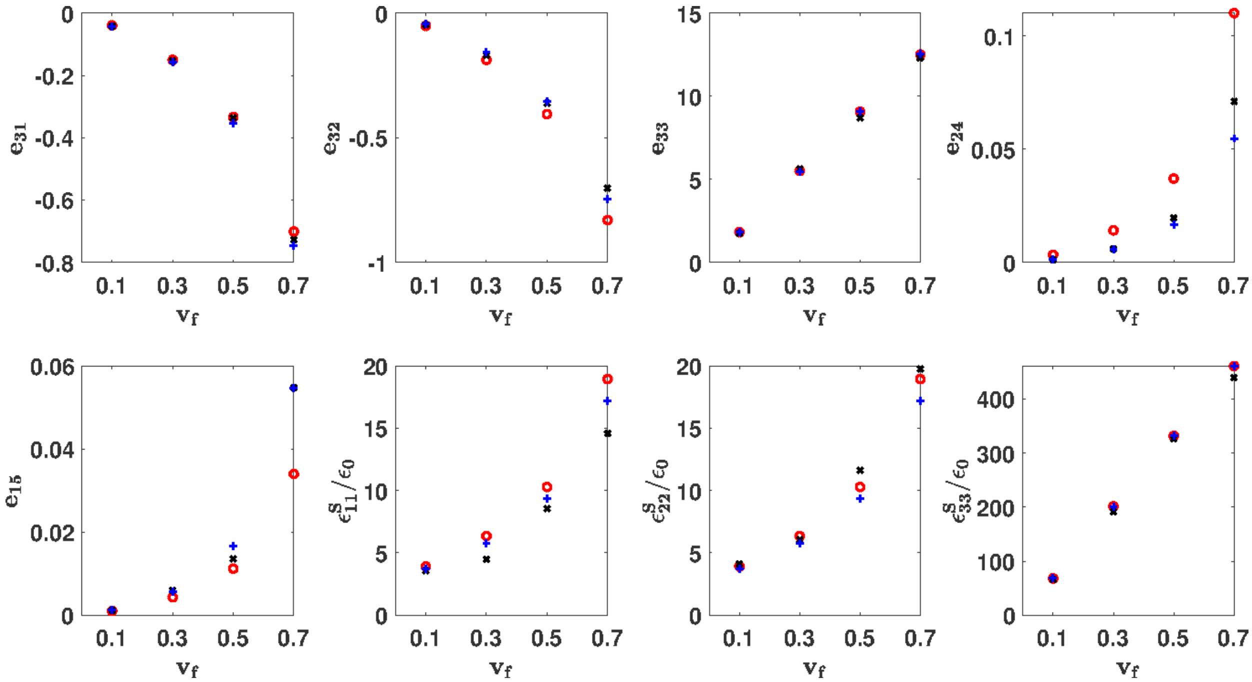

FIG. 6. Homogenized piezoelectric (in $C.m^{-2}$) and dielectric coefficients (in $/\epsilon_0$) from the present study represented with the black cross for mm2-structure and blue plus sign for 4mm-structure. Results from FFT method is also added with red circle for mm2-structure. Variations are according to volume fraction v_f.

C. Simplification for an experimental homogenization: example of the 4mm-structure

In order to apply the present method to an experimental setup, particular effort has to be expended on the acquisition of 13PC slowness curves for the 3 planes of interest. In fact, in the theoretical methodology (general case), 13PC slowness curves were calculated using FEM in all directions at incremental steps of 1°. Unfortunately, measurements made this way, are extremely laborious but also unnecessary. Rather the objective is to find a trade-off between the number of measurements and the accuracy of the deduced effective tensors. The example of a 4mm-structure was chosen here because it is the most frequently used in practice.

As shown in section III A, specific directions are necessary to determine several constants analytically: for the 4mm-structure in the XY-plane, x-direction and $(45, 90)$-direction provide the constants $\overline{c}^E_{11}$, $\overline{c}^E_{12}$, $\overline{c}^E_{66}$ and the z-direction in the XZ-plane (or YZ-plane) brings the $\overline{c}^E_{44}$ value. Hence, these three directions are retained. Moreover, the fitting process (section III B) for the 4mm-structure has to determine the constants $\overline{c}^E_{13}$, $\overline{c}^E_{33}$, $\overline{e}_{15}$, $\overline{e}_{31}$, $\overline{e}_{33}$, $\overline{\epsilon}_{11}$ and $\overline{\epsilon}_{33}$. These constants appear in two specific directions of the XZ-plane (or YZ-plane):

- z-direction (already retained at step 1) for $\overline{c}^E_{33}$, $\overline{e}_{33}$ and $\overline{\epsilon}_{33}$ on the QL mode,
- and $(0, 45)$- or $(90, 45)$-direction for the rest on the QL and QT1 modes.

To ensure the validity of the effective parameters obtained using a reduced number of directions (reduced case), the relative difference between these values and the general case must not exceed 5%. This limit was arbitrarily chosen. Using only the $(0, 45)$-direction in addition to the three ($(0, 90)$, $(45, 90)$ and $(0, 0)$) for the analytical determination, results were compared with the general case (45 directions in 2 planes = 90 directions) and, were generally correct for all volume fractions (10%, 30%, 50% and 70%) with relative differences lower than 10% except for e_{15} due to difficulties explained in section IV A. In table III, the 30% volume fraction case is presented because it is the case which exhibits the highest relative differences. Only the fitted parameters are presented because parameter determined by analytical method is, by definition, always equal. It is noticeable that the final results deteriorate with relative differences of 93% for the e_{31} value and 72% for e_{15}. This also confirms that substantial experimental information is lost, with a reduction in angles. The objective then is to add a few more experimental data to see whether the accuracy of the final results can be improved.

TABLE III. Effective elastic $\overline{c}^E$ (GPa), piezoelectric $\overline{e}$ (C.m^{-2}) and dielectric $\overline{\epsilon}^S$ $(/\epsilon_0)$ constant of 4mm-structure (v_f =30%).

Properties	general case	reduced cases			
	90 directions	4 directions (rel. diff. %)		6 directions (rel. diff. %)	
c_{13}^E	6,01	6,71	(12)	6,00	(0.1)
c_{33}^E	28,08	26,68	(4)	27,87	(1)
e_{15}	3,54e-4	0.0001	(72)	1,78e-4	(30)
e_{31}	-0.14	-0,27	(93)	-0,14	(0)
e_{33}	5,35	5,52	(3)	5,25	(2)
$\epsilon_{11}^S/\epsilon_0$	5,81	6,08	(5)	5,56	(4)
$\epsilon_{33}^S/\epsilon_0$	202	194	(4)	200	(1)

For the algorithm, there is a lack of accuracy evaluated on constants calculated from the QL and QT1 modes in $(0, 45)$-direction. Consequently, two additional directions: $(0, 30)$- and $(0, 60)$-directions are considered. In this way, the algorithm is better able to reveal the velocity variations in this plane. These results are also shown in table III (6 directions).

As expected, relative differences declined with a maximum of 4% (except for the e_{15} value). With these three cases, the logical trend of increasing accuracy, coupled with the increase in measured directions, are highlighted. Finally, when angle reductions are applied to the experimental setup, the user is obliged to consider choosing a trade-off between the number of measured directions and accuracy of the effective constants.

V. CONCLUSION

A method based on wave propagation was successfully implemented to determine the effective electroelastic moduli of 1-3 piezocomposites. Slowness curves in several planes were used to identify all the parameters, whose, Christoffel tensors were analytically expressed. This procedure was performed in two main steps. First, several elastic constants (listed in table II with stars) in particular directions were directly determinated using the quasi-longitudinal and two quasi-transversal modes. Second, to complete generation of the effective data (constants without star in table II) a fitting process using the Nelder-Mead algorithm was performed. In this study, two piezoelectric rod shapes (square and right-triangle) that can be designed by the well-known "Dice and Fill" method were selected. These two configurations belong to 4mm and mm2 symmetry class, respectively. For the second and most general case, requiring the determination of 17 constants, 10 ($\overline{c}^E_{11}$, $\overline{c}^E_{12}$, $\overline{c}^E_{13}$, $\overline{c}^E_{22}$, $\overline{c}^E_{33}$, $\overline{c}^E_{44}$, $\overline{c}^E_{55}$, $\overline{c}^E_{66}$, $\overline{e}_{31}$ and $\overline{\epsilon}^S_{33}$) were obtained with an accuracy of less than 2%. Larger differences were obtained for the two dielectric and two piezoelectric constants ($\overline{e}_{24}$, $\overline{e}_{15}$, $\overline{\epsilon}^S_{11}$ and $\overline{\epsilon}^S_{22}$) however, these values have limited influence for most applications using thickness or flexural modes. To validate our approach, the results were compared with a Fourier transform-based numerical homogenization scheme for quasi-static conditions. The idea behind this development was to use this method in *operating conditions* for 1-3 piezocomposite while also taking into account variations in properties, as compared to the original materials database of each phase, appearing in the fabrication process. From a practical point of view, we showed that with only 7 carefully chosen directions of propagation, the entire database of 1-3 piezocomposite with 4mm symmetry can be determined. Future applications can be guided by adaptation of this method to 1-3 piezocomposite for a given thickness and lateral dimensions. Here, direct measurements of propagative Lamb waves are more suitable. Just as the method described for volume waves, dispersion curves corresponding to the first three symmetric and antisymmetric theoretical Lamb modes will be exploited. Specific electrode designs on 1-3 piezocomposite will be used to generate modes in a particular direction and scanning laser vibrometer can be used to measure normal displacements at the surface specimen to deduce experimental disperse curve[49]. This new objective is now underway.

ACKNOWLEDGMENTS

This work was supported by the French Research Agency (ANR HEcATE 14-CE07-0028).

APPENDIX A:

For a piezoelectric material with mm2-symmetry, piezoelectric Christoffel tensor's components are:

$$\overline{\Gamma}_{11} = c_{11}^E n_1^2 + c_{66}^E n_2^2 + c_{55}^E n_3^2 + \frac{(e_{15}+e_{31})^2 n_1^2 n_3^2}{\epsilon_{11}^S n_1^2 + \epsilon_{22}^S n_2^2 + \epsilon_{33}^S n_3^2}, \tag{A1}$$

$$\overline{\Gamma}_{12} = (c_{12}^E + c_{66}^E)n_1n_2 + \frac{(e_{15} + e_{31})n_1n_3(e_{24} + e_{32})n_2n_3}{\epsilon_{11}^S n_1^2 + \epsilon_{22}^S n_2^2 + \epsilon_{33}^S n_3^2}, \tag{A2}$$

$$\overline{\Gamma}_{13} = (c_{13}^E + c_{55}^E)n_1n_3 + \frac{(e_{15} + e_{31})n_1n_3(e_{15}n_1^2 + e_{24}n_2^2 + e_{33}n_3^2)}{\epsilon_{11}^S n_1^2 + \epsilon_{22}^S n_2^2 + \epsilon_{33}^S n_3^2}, \tag{A3}$$

$$\overline{\Gamma}_{22} = c_{66}^E n_1^2 + c_{22}^E n_2^2 + c_{44}^E n_3^2 + \frac{(e_{24} + e_{32})^2 n_2^2 n_3^2}{\epsilon_{11}^S n_1^2 + \epsilon_{22}^S n_2^2 + \epsilon_{33}^S n_3^2}, \tag{A4}$$

$$\overline{\Gamma}_{23} = (c_{23}^E + c_{44}^E)n_2n_3 + \frac{(e_{24} + e_{32})n_2n_3(e_{15}n_1^2 + e_{24}n_2^2 + e_{33}n_3^2)}{\epsilon_{11}^S n_1^2 + \epsilon_{22}^S n_2^2 + \epsilon_{33}^S n_3^2}, \tag{A5}$$

$$\overline{\Gamma}_{33} = c_{55}^E n_1^2 + c_{44}^E n_2^2 + c_{33}^E n_3^2 + \frac{(e_{15}n_1^2 + e_{24}n_2^2 + e_{33}n_3^2)^2}{\epsilon_{11}^S n_1^2 + \epsilon_{22}^S n_2^2 + \epsilon_{33}^S n_3^2}. \tag{A6}$$

APPENDIX B:

Expression of the six velocities for XZ-plane and YZ-plane according to the solutions of equation 7:

- XZ-plane:

$$n_1 = sin\theta \ , \ n_2 = 0 \ , \ n_3 = cos\theta$$

Solutions are:

$$\begin{cases} V_{QT2}^2 = \frac{\overline{\Gamma}_{22}}{\rho} \\ V_{QL,QT1}^2 \pm = \frac{\overline{\Gamma}_{11} + \overline{\Gamma}_{33} \pm \sqrt{(\overline{\Gamma}_{11} + \overline{\Gamma}_{33})^2 - 4(\overline{\Gamma}_{11}\overline{\Gamma}_{33} - \overline{\Gamma}_{13}^2)}}{2\rho} \end{cases} \tag{B1}$$

- YZ-plane:

$$n_1 = 0 \ , \ n_2 = sin\theta \ , \ n_3 = cos\theta$$

$$\begin{cases} V_{QT2}^2 = \frac{\overline{\Gamma}_{11}}{\rho} \\ V_{QL,QT1}^2 \pm = \frac{\overline{\Gamma}_{22}+\overline{\Gamma}_{33}\pm\sqrt{(\overline{\Gamma}_{22}+\overline{\Gamma}_{33})^2-4(\overline{\Gamma}_{22}\overline{\Gamma}_{33}-\overline{\Gamma}_{23}^2)}}{2\rho} \end{cases} \tag{B2}$$

APPENDIX C:

Considering the unit-cell Ω of a periodic piezoelectric media, the quasi-static heterogeneous local problem reads, $\forall \mathbf{x} \in \Omega$,

$$\begin{cases} \operatorname{curl}(\operatorname{curl}^{\mathrm{T}} \mathbf{S}(\mathbf{x})) = \mathbf{0}, \quad \operatorname{div} \mathbf{T}(\mathbf{x}) = \mathbf{0}, \\ \operatorname{curl} \mathbf{E}(\mathbf{x}) = \mathbf{0}, \quad \operatorname{div} \mathbf{D}(\mathbf{x}) = \mathbf{0}, \end{cases} \tag{C1}$$

with coupled constitutive equations (1)

$$\mathbf{T} = \mathbf{c}^E : \mathbf{S} - \mathbf{e}^{\mathrm{T}}.\mathbf{E}, \quad \mathbf{D} = \boldsymbol{\epsilon}^S.\mathbf{E} + \mathbf{e} : \mathbf{S} \tag{C2}$$

and imposed periodicity conditions on the local fields on the boundary of the unit-cell Ω. Making use of the Green functions method, the solution fields are expressible as coupled Lippmann-Schwinger equations[39]

$$\begin{cases} \mathbf{S}(\mathbf{x}) = \langle \mathbf{S} \rangle_\Omega - \boldsymbol{\Gamma}^0 * \boldsymbol{\tau}(\mathbf{x}) \\ \mathbf{E}(\mathbf{x}) = \langle \mathbf{E} \rangle_\Omega - \boldsymbol{\Delta}^0 * \mathbf{P}(\mathbf{x}) \end{cases} \tag{C3}$$

with $\boldsymbol{\Gamma}^0$ and $\boldsymbol{\Delta}^0$ the Green operators corresponding to a uniform reference material with elastic tensor $\mathbf{c}^0$ and dielectric tensor $\boldsymbol{\epsilon}^0$. $\langle . \rangle_\Omega$ indicate the volume average over the unit-cell.

The fields $\boldsymbol{\tau}$ and $\mathbf{P}$ are given by

$$\begin{cases} \boldsymbol{\tau}(\mathbf{x}) = (\mathbf{c}^E(\mathbf{x}) - \mathbf{c}^0) : \mathbf{S}(\mathbf{x}) - \mathbf{e}^{\mathrm{T}}(\mathbf{x}).\mathbf{E}(\mathbf{x}) \\ \\ \mathbf{P}(\mathbf{x}) = \mathbf{e}(\mathbf{x}) : \mathbf{S}(\mathbf{x}) + (\epsilon^S(\mathbf{x}) - \boldsymbol{\epsilon}^0).\mathbf{E}(\mathbf{x}). \end{cases} \tag{C4}$$

The solution fields (C3) can be expressed in Fourier space and the problem is solved using an adequate iterative procedure[38,39]. The effective electroelastic coefficients tensors $\widetilde{\mathbf{c}}^E$, $\widetilde{\mathbf{e}}$ and $\widetilde{\boldsymbol{\epsilon}}^S$ are defined by

$$\langle \mathbf{T} \rangle_\Omega = \widetilde{\mathbf{c}}^E : \langle \mathbf{S} \rangle_\Omega - \widetilde{\mathbf{e}}^{\mathrm{T}}.\langle \mathbf{E} \rangle_\Omega\,, \quad \langle \mathbf{D} \rangle_\Omega = \widetilde{\boldsymbol{\epsilon}}^S.\langle \mathbf{E} \rangle_\Omega + \widetilde{\mathbf{e}} : \langle \mathbf{S} \rangle_\Omega \tag{C5}$$

References

[1] R. Newnham, D. Skinner, and L. Cross, "Connectivity and piezoelectric-pyroelectric composites," Materials Research Bulletin **13**(5), 525–536 (1978) https://linkinghub.elsevier.com/retrieve/pii/0025540878901617 doi: 10.1016/0025-5408(78)90161-7.

[2] W. A. Smith and B. A. Auld, "Modeling 1-3 composite piezoelectrics: thickness-mode oscillations.," IEEE transactions on ultrasonics, ferroelectrics, and frequency control **38**(1), 40–7 (1991) http://www.ncbi.nlm.nih.gov/pubmed/18267555 doi: 10.1109/58.67833.

[3] M. Lethiecq, F. Levassort, D. Certon, and L. P. Tran-Huu-Hue, "Piezoelectric Transducer Design for Medical Diagnosis and NDE," in *Piezoelectric and Acoustic Materials for Transducer Applications* (Springer US, Boston, MA, 2008), pp. 191–215, http://link.springer.com/10.1007/978-0-387-76540-2{_}10, doi: 10.1007/978-0-387-76540-2_10.

[4] W. Voigt, “Ueber die Beziehung zwischen den beiden Elasticitätsconstanten isotroper Körper,” Annalen der Physik **274**(12), 573–587 (1889) http://doi.wiley.com/10.1002/andp.18892741206 doi: 10.1002/andp.18892741206.

[5] A. Reuss, “Berechnung der Fließgrenze von Mischkristallen auf Grund der Plastizitätsbedingung für Einkristalle .,” ZAMM - Zeitschrift für Angewandte Mathematik und Mechanik **9**(1), 49–58 (1929) http://doi.wiley.com/10.1002/zamm.19290090104 doi: 10.1002/zamm.19290090104.

[6] P. Bisegna and R. Luciano, “Variational bounds for the overall properties of piezoelectric composites,” J. Mech. Phys. Solids **44**, 583–602 (1996).

[7] H. Banno, “Theoretical Equations for Dielectric and Piezoelectric Properties of Ferroelectric Composites Based on Modified Cubes Model,” Japanese Journal of Applied Physics **24**(S2), 445 (1985) http://stacks.iop.org/1347-4065/24/445 doi: 10.7567/JJAPS.24S2.445.

[8] K. Hashimoto and M. Yarnaguchi, “Elastic, Piezoelectric and Dielectric Properties of Composite Materials,” in *IEEE 1986 Ultrasonics Symposium*, IEEE (1986), pp. 697–702, http://ieeexplore.ieee.org/document/1535764/, doi: 10.1109/ULTSYM.1986.198824.

[9] H. Chan and J. Unsworth, “Simple model for piezoelectric ceramic/polymer 1-3 composites used in ultrasonic transducer applications,” IEEE Transactions on Ultrasonics, Ferroelectrics and Frequency Control **36**(4), 434–441 (1989) http://ieeexplore.ieee.org/document/31780/ doi: 10.1109/58.31780.

[10]H. Banno, “Theoretical Equations for Dielectric, Piezoelectric and Elastic Properties of a 0–3 Composite Based on Modified Cubes Model–A General Solution–,” Japanese Journal of Applied Physics **28**(S2), 190 (1989) http://stacks.iop.org/1347-4065/28/190 doi: 10.7567/JJAPS.28S2.190.

[11]F. Levassort, M. Lethiecq, D. Certon, and F. Patat, “A matrix method for modeling electroelastic moduli of 0-3 piezo-composites,” IEEE Transactions on Ultrasonics, Ferroelectrics and Frequency Control **44**(2), 445–452 (1997) http://ieeexplore.ieee.org/document/585129/ doi: 10.1109/58.585129.

[12]J. Eshelby, “The determination of the elastic field of an ellipsoidal inclusion, and related problems,” Proceedings of the Royal Society of London. Series A. Mathematical and Physical Sciences **241**(1226), 376–396 (1957) https://royalsocietypublishing.org/doi/10.1098/rspa.1957.0133 doi: 10.1098/rspa.1957.0133.

[13]W. Deeg, “The analysisof dislocation, crack, and inclusion problems in piezoelectric solids,” Ph.D. thesis, Standford University, 1980.

[14]M. Dunn and M. Taya, “An analysis of piezoelectric composite materials containing ellipsoidal inhomogeneities,” Proceedings of the Royal Society of London. Series A: Mathematical and Physical Sciences **443**(1918), 265–287 (1993) https://royalsocietypublishing.org/doi/10.1098/rspa.1993.0145 doi: 10.1098/rspa.1993.0145.

[15]T. Mori and K. Tanaka, "Average stress in matrix and average elastic energy of materials with misfitting inclusions," Acta Metallurgica **21**(5), 571–574 (1973) https://linkinghub.elsevier.com/retrieve/pii/0001616073900643 doi: 10.1016/0001-6160(73)90064-3.

[16]Y. Benveniste, "The determination of the elastic and electric fields in a piezoelectric inhomogeneity," Journal of Applied Physics **72**(3), 1086–1095 (1992) http://aip.scitation.org/doi/10.1063/1.351784 doi: 10.1063/1.351784.

[17]W. Biao, "Three-dimensional analysis of an ellipsoidal inclusion in a piezoelectric material," International Journal of Solids and Structures **29**(3), 293–308 (1992) https://linkinghub.elsevier.com/retrieve/pii/0020768392902014 doi: 10.1016/0020-7683(92)90201-4.

[18]H. Berger, S. Kari, U. Gabbert, R. Rodriguez-Ramos, R. Guinovart, J. A. Otero, and J. Bravo-Castillero, "An analytical and numerical approach for calculating effective material coefficients of piezoelectric fiber composites," International Journal of Solids and Structures **42**(21-22), 5692–5714 (2005) https://linkinghub.elsevier.com/retrieve/pii/S0020768305001277 doi: 10.1016/j.ijsolstr.2005.03.016.

[19]A. A. Bent and N. W. Hagood, "Piezoelectric Fiber Composites with Interdigitated Electrodes," Journal of Intelligent Material Systems and Structures **8**(11), 903–919 (1997) http://journals.sagepub.com/doi/10.1177/1045389X9700801101 doi: 10.1177/1045389X9700801101.

[20]C. Poizat and M. Sester, “Effective properties of composites with embedded piezoelectric fibres,” Computational Materials Science **16**(1-4), 89–97 (1999) https://linkinghub.elsevier.com/retrieve/pii/S0927025699000506 doi: 10.1016/S0927-0256(99)00050-6.

[21]H. E. Pettermann and S. Suresh, “A comprehensive unit cell model: a study of coupled effects in piezoelectric 1–3 composites,” International Journal of Solids and Structures **37**(39), 5447–5464 (2000) https://linkinghub.elsevier.com/retrieve/pii/S0020768399002243 doi: 10.1016/S0020-7683(99)00224-3.

[22]E. Lenglet, A.-C. Hladky-Hennion, and J.-C. Debus, “Numerical homogenization techniques applied to piezoelectric composites,” The Journal of the Acoustical Society of America **113**(2), 826–833 (2003) http://asa.scitation.org/doi/10.1121/1.1537710 doi: 10.1121/1.1537710.

[23]H. Berger, S. Kari, U. Gabbert, R. Rodriguez-Ramos, J. Bravo-Castillero, R. Guinovart-Diaz, F. J. Sabina, and G. A. Maugin, “Unit cell models of piezoelectric fiber composites for numerical and analytical calculation of effective properties,” Smart Materials and Structures **15**(2), 451–458 (2006) http://stacks.iop.org/0964-1726/15/i=2/a=026?key=crossref.9f57e8e0ef4a86f7fcf2693e6043 doi: 10.1088/0964-1726/15/2/026.

[24]T. Enab, “Evaluation of the Effective Electromechanical Properties of Unidirectional Piezocomposites Using Different Representative Volume Elements,” International Journal of Mechanical and Mechatronics Engineering **15**(2), 21–29 (2015).

[25]S. Kari, H. Berger, R. Rodriguez-Ramos, and U. Gabbert, "Numerical Evaluation of Effective Material Properties of Transversely Randomly Distributed Unidirectional Piezoelectric Fiber Composites," Journal of Intelligent Material Systems and Structures **18**(4), 361–372 (2007) http://journals.sagepub.com/doi/10.1177/1045389X06066293 doi: 10.1177/1045389X06066293.

[26]R. Kar-Gupta and T. A. Venkatesh, "Electromechanical response of 1-3 piezoelectric composites: Effect of poling characteristics," Journal of Applied Physics **98**(5), 054102 (2005) http://aip.scitation.org/doi/10.1063/1.2014933 doi: 10.1063/1.2014933.

[27]S. Aimmanee, and H. Asanuma, "Micromechanics-based predictions of effective properties of a 1-3 piezocomposite reinforced with hollow piezoelectric fibers," Mechanics of Advanced Materials and Structures **27**(22), 1873–1887 (2020) https://www.tandfonline.com/doi/full/10.1080/15376494.2018.1529842 doi: 10.1080/15376494.2018.1529842.

[28]Y. Zhang, L. Wang and L. Qin, "Equivalent parameter model of 1-3 piezocomposite with a sandwich polymer," Results in Physics **9**, 1256–1261 (2018) https://linkinghub.elsevier.com/retrieve/pii/S2211379717317515 doi: 10.1016/j.rinp.2018.04.046.

[29]H. Savakus, K. Klicker, and R. Newnham, "PZT-epoxy piezoelectric transducers: A simplified fabrication procedure," Materials Research Bulletin **16**(6), 677–680 (1981) http://linkinghub.elsevier.com/retrieve/pii/0025540881902671 doi: 10.1016/0025-5408(81)90267-1.

[30] R. Rouffaud, A.-C. Hladky-Hennion, and F. Levassort, “A combined genetic algorithm and finite element method for the determination of a practical elasto-electric set for 1-3 piezocomposite phases,” Ultrasonics **77** (2017) doi: 10.1016/j.ultras.2017.02.015.

[31] Y. C. Chu and S. I. Rokhlin, “Stability of determination of composite moduli from velocity data in planes of symmetry for weak and strong anisotropies,” The Journal of the Acoustical Society of America **95**(1), 213–225 (1994) http://asa.scitation.org/doi/10.1121/1.408378 doi: 10.1121/1.408378.

[32] C. Potel, J. de Belleval, and Y. Gargouri, “Floquet waves and classical plane waves in an anisotropic periodically multilayered medium: Application to the validity domain of homogenization,” The Journal of the Acoustical Society of America **97**(5), 2815–2825 (1995) http://asa.scitation.org/doi/10.1121/1.411849 doi: 10.1121/1.411849.

[33] L. Wang and S. I. Rokhlin, “Floquet wave homogenization of periodic anisotropic media,” The Journal of the Acoustical Society of America **112**(1), 38–45 (2002) http://asa.scitation.org/doi/10.1121/1.1488942 doi: 10.1121/1.1488942.

[34] M. Wilm, S. Ballandras, V. Laude, and T. Pastureaud, “A full 3D plane-wave-expansion model for 1-3 piezoelectric composite structures,” The Journal of the Acoustical Society of America **112**(3), 943–952 (2002) http://asa.scitation.org/doi/10.1121/1.1496081 doi: 10.1121/1.1496081.

[35] G. Ferin, D. Certon, N. Felix, and F. Patat, “Experimental and theoretical determination of 1–3 piezocomposite electroacoustic tensor,” Ultrasonics **44**, e763–e772 (2006) https://linkinghub.elsevier.com/retrieve/pii/S0041624X06001259

doi: 10.1016/j.ultras.2006.05.090.

[36] P. Langlet, A. Hladky-Hennion, and J. Decarpigny, "Analysis of the propagation of plane acoustic waves in passive periodic materials using the finite element method," The Journal of the Acoustical Society of America **98**(5), 2792–2800 (1995) http://asa.scitation.org/doi/10.1121/1.413244 doi: 10.1121/1.413244.

[37] H. Moulinec and P. Suquet, "A numerical method for computing the overall response of nonlinear composites with complex microstructure," Computer Methods in Applied Mechanics and Engineering **157**(1-2), 69–94 (1998) https://linkinghub.elsevier.com/retrieve/pii/S0045782597002181 doi: 10.1016/S0045-7825(97)00218-1.

[38] R. Brenner, "Numerical computation of the response of piezoelectric composites using fourier transform," Physical Review B **79**(18), 184106 (2009) https://link.aps.org/doi/10.1103/PhysRevB.79.184106 doi: 10.1103/PhysRevB.79.184106.

[39] R. Brenner, "Computational approach for composite materials with coupled constitutive laws," Zeitschrift für angewandte Mathematik und Physik **61**, 919–927,1420–9039 (2010).

[40] R. Brenner, J. Bravo-Castillero, and D. M. Léon, "Investigation of the effective response of 2-1-2 piezoelectric composites," Procedia IUTAM **3**, 292–300 (2012).

[41] T. Ikeda, *Fundamentals of Piezoelectricity* (Oxford University Press, New York, 1996).

[42] D. Royer and E. Dieulesaint, *Elastic Waves in Solids I: Free and Guided Propagation* (Springer-Verlag Berlin, 1999).

[43]McGrawHill, *American Institute of Physics Handbook*, 2ème éditi ed. (1963).

[44]M. Pham Thi, A.-C. Hladky-Hennion, H. L. Khanh, L.-P. Tran-Huu-Hue, M. Lethiecq, and F. Levassort, "Large area 0-3 and 1-3 piezoelectric composites based on single crystal PMN-PT for transducer applications," Physics Procedia **3**(1), 897–904 (2010) http://linkinghub.elsevier.com/retrieve/pii/S1875389210001161 doi: 10.1016/j.phpro.2010.01.115.

[45]J. A. Brown, E. Cherin, J. H. Yin, and F. S. Foster, "Fabrication and Performance of High-Frequency Composite Transducers with Triangular-Pillar Geometry," Ieee Transactions on Ultrasonics Ferroelectrics and Frequency Control **56**(4), 827–836 (2009) doi: 10.1109/tuffc.2009.1106.

[46]ISEN, "ATILA, Finite-Element Software Package for the analysis of 2D & 3D structures based on smart materials" (2010).

[47]A. Balé, "Homogénéisation et caractérisation de matériaux multiphasiques piézoélectriques (composites de connectivité 1-3 et céramiques texturées) pour les transducteurs ultrasonores sans plomb," Ph.D. thesis, University of Tours, 2019.

[48]J. Nelder and R. Mead, "A simplex method for function minimization," Computer Journal **7**(4), 308–313 (1965).

[49]J. Guyonvarch, D. Certon, L. Ratsimandresey, F. Patat, and M. Lethiecq, "Response of bare 1–3 piezocomposite array to localized electrical excitation," The Journal of the Acoustical Society of America **117**(1), 200–209 (2005) http://asa.scitation.org/doi/10.1121/1.1829259 doi: 10.1121/1.1829259.